ACS Photonics

Letter

Cite This: ACS Photonics 2018, 5, 1188−1195

Metal Nanoparticle Array as a Tunable Refractive Index Material over Broad Visible and Infrared Wavelengths

Reehyang Kim,[†] Kyungjae Chung,[‡] Ju Young Kim,[§] Yunyong Nam,[†] Sang-Hee Ko Park,[†] and Jonghwa Shin*[,†]

[†]Department of Materials Science and Engineering, Korea Advanced Institute of Science and Technology, 291 Daehak-ro, Yuseong-gu, Daejeon, 34141, Republic of Korea

[‡]Samsung Electronics, 1 Samsungjeonja-ro, Hwaseong-si, Gyeongi-do 18448, Republic of Korea

[§]Electronics and Telecommunications Research Institute, 218 Gajeong-ro, Yuseong-gu, Daejeon, 34129, Republic of Korea

Supporting Information

ABSTRACT: Common materials show a limited range of refractive indices over the visible and infrared wavelengths, and their values are not easily tunable once the material is chosen. Here, self-assembled metal nanoparticle arrays are proposed as an effective optical material with a large range of possible refractive indices that are nearly dispersionless over broad wavelength ranges. The material can be potentially fabricated over a large curved surface, and the resulting index is even more tunable by various postprocessing methods, such as material substitution or mechanical stretching. We achieve the highest refractive index of 5.0 at resonance in the visible, exceeding 4.2 over a broadband wavelength regime out of resonance. The key differences from previous studies of self-assembled metal particle arrays are the consideration of the diamagnetic effect and the careful choice of the ligands, which determine the gaps between particles. The sensitivity of the effective index to the size and material of the gap region allows the use of particle arrays also as an optical sensor of mechanical strain or the densities of analyte solutions with very small reaction volumes.

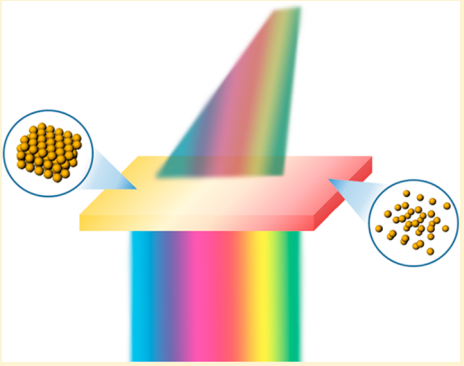

KEYWORDS: *refractive index, tunable metamaterial, metal nanoparticles, self-assembly, effective medium*

Over the last few decades, there has been remarkable progress in the field of nanoparticle synthesis and in related utilizations.[1−5] In particular, metal nanoparticles have attracted tremendous amounts of attention due to their novel properties, which differ greatly from those of the bulk.[6−8] Diverse synthesis methods have been studied to prepare nanoparticles with a variety of materials and shapes,[1−3] as have different methods of arranging the synthesized nanoparticles into well-ordered arrays.[4,5] As a result of these extensive studies, metal nanoparticles are being applied to a wide range of fields, including catalysis,[9] photovoltaics,[10] therapeutics,[11] and plasmonics.[12] In the case of plasmonics, the main effect typically comes from the fact that metallic nanoparticles can produce local hot spots of high electric fields when illuminated by light with appropriate wavelengths and polarizations. Surface-enhanced Raman scattering (SERS) and resonance sensing are among the many possible applications of this effect.[13−15]

On the other hand, there have been many studies of metamaterials to overcome the natural limitations of the refractive indices ($n = (\varepsilon \cdot \mu)^{1/2}$, where ε and μ are the relative electric permittivity and magnetic permeability, respectively). As the refractive index is arguably the most basic and important optical property of materials, governing physical phenomena ranging from the propagation and refraction to the emission and absorption of light, enlarging the possible range of indices can lead to much improved performance of existing devices as well as the emergence of novel optical devices. For example, negative indices[16−18] and near-zero indices[19−21] have been realized by introducing artificial resonances, with potential applications including invisibility cloaks, super lenses, and ultrathin absorbers. However, the refractive indices in these cases are highly dispersive, showing strong dependence on the wavelength, which is unavoidable due to the direct reliance on the plasmonic resonance, an issue that hinders further practical applications. To overcome this fundamental difficulty, designs based on a quasi-static boundary condition were recently utilized to achieve a high refractive index over a broad wavelength range.[22−25] If one can realize broadband materials with a high refractive index for visible and infrared wavelengths with simple, lithography-free fabrication processes, it would be natural to expect diverse practical applications, such as super-resolution imaging, immersion lenses for lithography, compact optical modulators, and solar energy converters. Several researchers have attempted to control the refractive index

Received: December 7, 2017
Published: March 8, 2018

Downloaded via KOREA ADVANCED INST SCI AND TECHLGY on December 19, 2019 at 09:03:10 (UTC).
See https://pubs.acs.org/sharingguidelines for options on how to legitimately share published articles.

© 2018 American Chemical Society

DOI: 10.1021/acsphotonics.7b01497
ACS Photonics 2018, 5, 1188−1195

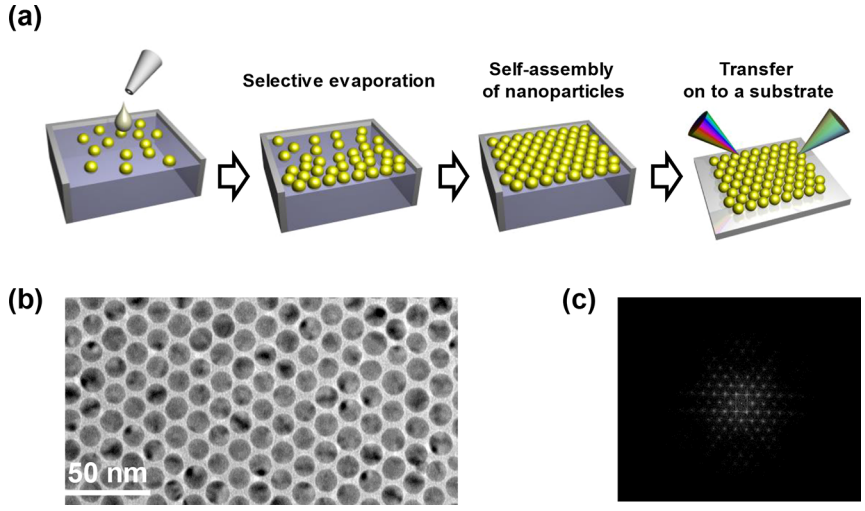

Figure 1. (a) Schematic of the fabrication procedure for the effective optical material. The mixture of gold nanoparticles, hexane, and toluene is spread on the surface of water. With a careful choice of the volume ratio of two solvents and proper design of the evaporation apparatus, gold nanoparticles can be self-assembled into a well-ordered array on the water surface. The self-assembled nanoparticle array is transferred to a substrate. (b) TEM image of self-assembled arrays of gold nanoparticles on a copper grid. (c) Two-dimensional Fourier transform of (b).

using nanoparticles,[26−35] but broadband high refractive indices have yet to be realized.

In this paper, we demonstrate broadband optical materials with a high refractive index with self-assembled metal nanoparticle arrays that are further tunable by applying atomic layer deposition (ALD) or with a stretchable substrate. We achieve refractive indices as high as 5 at the resonance wavelength and 4.2 over the broadband wavelength regime out of resonance. The proposed structure does not require complicated or advanced fabrication steps such as nanoscale lithography, and it can be realized by a self-assembly method. In addition, the fabrication method does not require a substrate, and the resulting array can be transferred to diverse substrates, including curved or corrugated substrates, opening the possibility for integration with other devices. We analyze the optical properties of the fabricated structures with a spectroscopic ellipsometer and compare these outcomes to predictions by numerical calculations based on a finite difference time domain (FDTD) method.

The fabrication steps start with the synthesis of hydrophobic gold nanoparticles encapsulated by a thin layer of oleylamine.[2] The synthesized gold nanoparticles, initially dispersed in hexane, are diluted by a mixture of toluene and hexane (volume ratio 1:2).[5] The mixture is spread on top of deionized water in a glass Petri dish, as illustrated in Figure 1a. Three quarters of the Petri dish is covered by a glass slide to control the evaporation of the organic solvents. Using the difference in the evaporation rates between toluene and hexane, monolayers of gold nanoparticles are fabricated, floating on the deionized water. The self-assembled gold nanoparticle monolayers are then transferred to diverse substrates via a method analogous to hydrographic printing,[36] which is commercially used to decorate objects with complex curved surfaces, such as vehicle wheels. The fabricated gold nanoparticle monolayers are observed by transmission electron microscopy (TEM), as depicted in Figure 1b. In the TEM image, the gold nanoparticles form a well-aligned hexagonal array. Moreover, the Fourier transformed image in Figure 1c shows a clear hexagonal array of gold nanoparticles. On the basis of these analyses, we determined that the average size of the gold nanoparticles is 11.5 ± 1.2 nm and the gap distance between the neighboring two gold nanoparticles is 2 nm. This gap distance can be controlled by using gold nanoparticles with different encapsulations because it is double the thickness of the encapsulation layer. In the Supporting Information, there are images of a gold nanoparticle array observed by an optical microscope and a scanning electron microscope (SEM) at various magnifications.

In order to obtain a high refractive index in the optical regime, we previously proposed a new optical effective medium theory for arrays of metal nanoparticles.[37] It was proved that the large difference between the Thomas−Fermi screening length of longitudinal electric fields and the penetration depth (skin depth) of transverse electromagnetic fields can be exploited to achieve a high index in the visible range. In this system, the permittivity (ε) is enhanced because the electric field is confined to the narrow dielectric gap region between gold nanoparticles, and the permeability (μ) does not decrease because the diamagnetic effect is negligible due to the small size of the gold nanoparticles compared to the skin depth. The refractive index is determined by the product of the permittivity and permeability, implying that we can control the refractive index. In our previous paper,[37] the effects of metal nanoparticle size and gap distance on the effective refractive index are extensively studied. Kim et al. demonstrated a high refractive index at an optical frequency using block copolymer lithography.[25] While Kim's approach is also potentially applicable to large areas, our single-step direct assembly approach does not necessitate a metal deposition and lift-off process in a vacuum chamber and allows much finer control on the gap size simply by choosing a proper encapsulation layer.

In Figure 2a (black line), the effective refractive index of a monolayer gold nanoparticle optical material is analyzed by spectroscopic ellipsometry. Near a resonance wavelength of 660 nm, the real part of the refractive index has a maximum value of 4.22. This is from a representative sample, and we measured 10 samples at 40 positions with an average maximum value of 4.205 with a standard deviation of 0.194 (Supporting Information S2). At longer wavelengths, the effective index saturates to a long-wavelength asymptotic value of 2.80 with a

DOI: 10.1021/acsphotonics.7b01497
ACS Photonics 2018, 5, 1188−1195

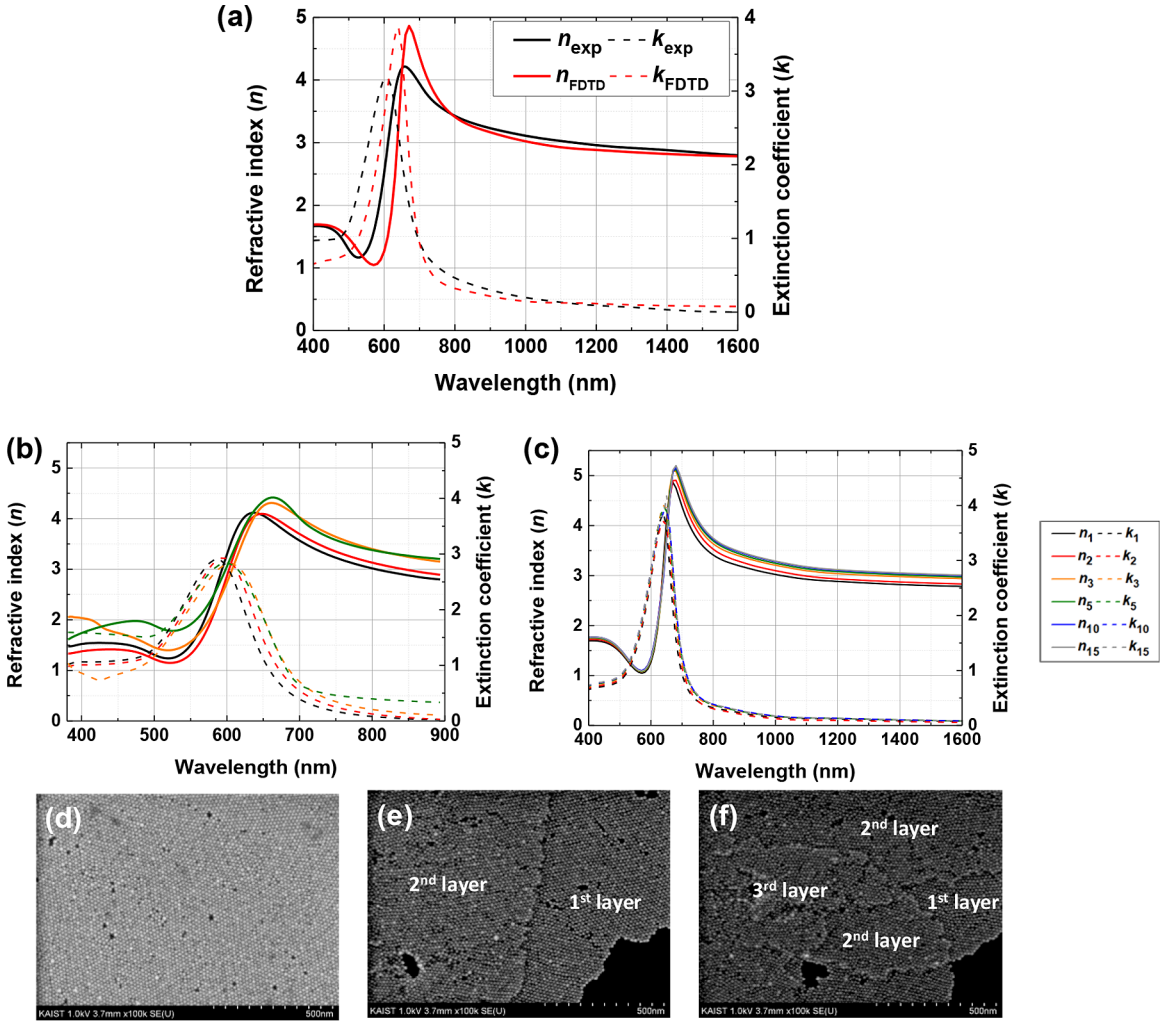

Figure 2. (a) Effective refractive indices of the effective optical material made of self-assembled gold nanoparticles measured by a spectroscopic ellipsometer (black) and compared to the predicted values from numerical simulations (red). The solid line stands for the real part of refractive index *n*, and the dashed line is for the imaginary part of the index, also known as the extinction coefficient *k*. (b) Effective refractive index measured for multilayer samples to check the consistency. The black, red, orange, and green lines stand for the result of one, two, three, and five layers of the effective optical material, respectively. (c) Numerically calculated refractive index for different numbers of layers. (d–f) Scanning electron microscope image for multilayers of the effective optical material.

negligible imaginary part, as predicted by our effective medium theory.[37] The numerical calculation result for a perfect monolayer of hexagonally close-packed spherical gold nanoparticles with a dielectric encapsulation layer is also plotted in Figure 2a for comparison (red lines). It is known that the electric permittivity of metallic nanoparticles differs from the bulk value due to surface-induced factors;[38] therefore, the size-dependent permittivity of gold nanoparticles is considered in the numerical calculations. The numerical results show good agreement with the experimental results, demonstrating a prominent peak near a wavelength of 670 nm and a nearly identical long-wavelength asymptotic value. The main difference is that the experimentally observed shape for the index peak is lower and broader than that in the numerical simulations. This is attributed to the inhomogeneous broadening due to the size dispersion of synthesized gold nanoparticles and imperfections in their hexagonal arrangement. The polydispersity results in slight variations of the actual resonant wavelength, and the experimentally observed data are a spatial average due to the broad optical beam used for the ellipsometry measurements. The polydispersity-induced peak broadening may be beneficial in applications in which the frequency dispersion of the effective index should be minimized. As the control simulations, we added numerical calculation results for various nanoparticle arrays, such as a resonance-based gold spheroid array or dielectric nanoparticle array, to compare effective refractive index enhancement in Supporting Information S3.

The self-assembled gold nanoparticle optical material can be considered as a truly volumetric effective material rather than a 2D-like metasurface, as the effective index remains consistent if the thickness of the material is increased by the deposition of multiple layers (Figure 2b). The effective refractive index saturates to an asymptotic curve for thicker samples with more than three layers. One can observe that the effective index for a five-layer sample is nearly indistinguishable from that of a 10- or 15-layer sample at all wavelengths considered (Figure 2c). This confirms that the proposed particle array system behaves as a conventional optical material with homogeneous material properties. There is a small initial increase in the index as the number of layers is increased from one to three; this is an expected result given the fact that a monolayer of metallic

DOI: 10.1021/acsphotonics.7b01497
ACS Photonics 2018, 5, 1188–1195

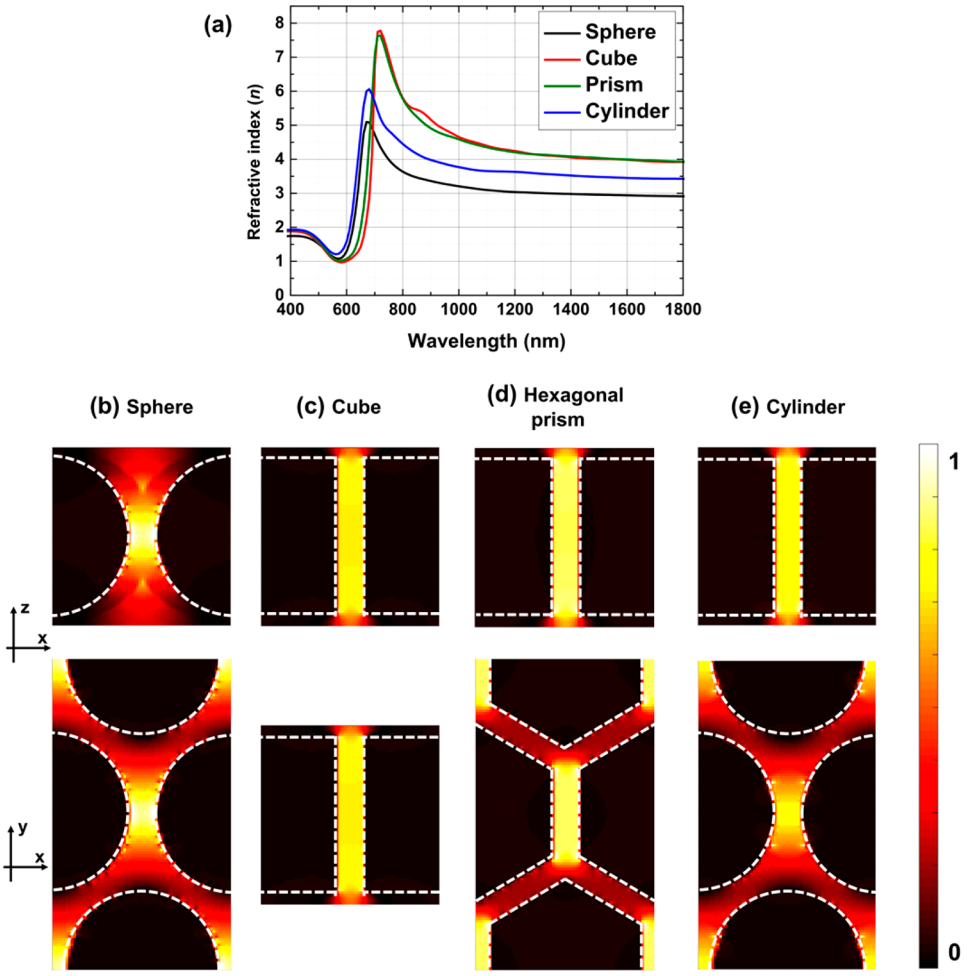

Figure 3. (a) Effective refractive indices for five layers of various shapes of gold nanoparticles calculated by FDTD simulations. The upper row of (b)−(e) is electric field distributions on the *x*-*o*-*z* plane for each case. The lower row of (b)−(e) is electric field distributions on the *x*-*o*-*y* plane for various shapes of nanoparticles. In all panels, the unit cell basis vector is 13.5 nm in length, and the minimum gap size between particles is 2 nm. The magnitude of the electric field is normalized by the maximum value in each profile.

particles is not one unit cell layer of the three-dimensional crystal. A true one-unit cell of a hexagonal close-packed crystal includes hemispherical particles from the layers below and above in addition to the entire sphere at the center (Supporting Information S4). Because the experimentally fabricated monolayer of particles lacks these partial particles, the effective permittivity and index are slightly lower due to the reduced capacitive effect. As the number of layers increases, the overall material properties should approach those of an infinite perfect crystal, and both the experimental and numerical results agree with this trend. The fabricated multilayers of gold nanoparticles are observed with an SEM (Figures 2d−f). These images were taken in the boundary regions, where the steps between different layers are clearly visible, thus allowing the counting of the number of layers. Atomic force microscopy measurement was also conducted for multilayers of a gold nanoparticle array (see Supporting Information).

The principle of broadband refractive index control can also be extended to other shapes and materials of metal nanoparticles. When the size of a metal particle is smaller than the skin depth, the effective permeability maintains unity ($\mu \approx 1$); thus, the effective refractive index is simply proportional to the square root of the effective permittivity ($n \approx (\varepsilon)^{1/2}$). The effective permittivity can be controlled by confining the electric field in the gap between metal particles.[37] This can be represented with the simple relationships of $n \propto (\varepsilon_h \cdot a/g)^{1/2}$, where ε_h is the permittivity of the surrounding polymeric material around the nanoparticle (in this case, the surrounding material is oleylamine[39,40]), a is the unit cell size of the nanoparticle array, and g is the gap distance between the nearest metal nanoparticles. Although we used spherical nanoparticles to demonstrate the design principle of this system, the principle applies to other particle shapes as well. In Figure 3b−e, the electric fields on the *x*-*o*-*z* and *x*-*o*-*y* planes are plotted for spheres, cubes, hexagonal prisms, and cylinders for comparison. All of these examples show a strong electric field confinement effect with an intense field in the narrow dielectric gap between the metallic structures and a negligible field inside the metallic region. While the images in Figure 3b−e were taken at a wavelength of 3000 nm, the field profiles remain nearly invariant at other wavelengths in the long-wavelength regime. Among these structures, faceted structures (cubes and hexagonal prisms) have intensified fields over a larger region compared to the other two (spheres and cylinders), which have curved surfaces. This difference results in a larger peak and a larger long-wavelength asymptotic value of the refractive index for the cubes and hexagonal prisms with the same a/g ratio, as presented in Figure 3a and Table 1. Specifically, for the cubic

DOI: 10.1021/acsphotonics.7b01497
ACS Photonics 2018, 5, 1188−1195

Table 1. Peak Wavelength and Effective Refractive Index of an Array of Various Gold Nanoparticles with Different Shapes

	sphere	cube	hexagonal polygon	cylinder
peak wavelength (nm)	670	720	720	680
maximum refractive index	5.08	7.75	7.62	5.60
refractive index at long wavelengths	2.91	3.92	3.91	3.15

particle array, the refractive index has a peak value as high as 7.8 at 720 nm and a long-wavelength value of 3.9. Despite these quantitative differences, the index control principle and the qualitative frequency dependence are common to all structures and also to other plasmonic materials such as silver and aluminum. In the Supporting Information, we include experimentally observed enhanced refractive index data for an array of silver nanoparticles with mixed shapes as an example.

Because the effective refractive index of the optical material in this study is $n \propto (\varepsilon_h \cdot a/g)^{1/2}$, one can further tune the fabricated optical material both by material substitution to vary ε_h (Figure 4a) and by mechanical deformation to vary a/g (Figure 4c). We change the encapsulation dielectric material (ε_h) surrounding the gold nanoparticle by ALD, as illustrated in Figure 4a. ALD can deposit materials conformally even between narrow gaps, and we verify that the dielectric material is successfully deposited between the nanoparticles by energy dispersive spectroscopy (EDS) mapping (see Supporting Information). Gold nanoparticles are encapsulated by oleylamine when fabricated, and we remove the oleylamine layer via an ultraviolet ozone treatment. We then coat the particles with TiO_2 or Al_2O_3 using ALD. When TiO_2 is deposited, given its higher ε_h than oleylamine,[41] the effective refractive index increases substantially from 3.45 to 4.25 at 900 nm, reaching a peak value of 5.00 at 725 nm. On the other hand, the deposition of Al_2O_3, which has a lower value of ε_h than oleylamine when the thickness is a few nanometers,[42,43] decreases the refractive index to 3.20 at 900 nm and blue-shifts the resonance (Figure 4b). These results are well matched with numerical calculations in Supporting Information S8. Given this sensitivity of the effective refractive index of the change in the refractive index of the encapsulation material, which is only one nanometer thick, the particle array can be used as an optical sensor with a very small detection volume if the surface is treated to bind to specific analytes (see Supporting Information).

For the mechanical approach of index tuning, we transfer the particle array to a flexible substrate and stretch the substrate to change the unit cell size a and the gap distance g. Because the metal particles are relatively rigid, their size b does not change upon substrate stretching. Thus, it is reasonable to assume that the amount of the increase in a is identical to the amount of the increase in g (note that $a = b + g$ is always satisfied). Thus, the a/g ratio decreases as the substrate is stretched. We stack the self-assembled gold nanoparticle array on a stretchable

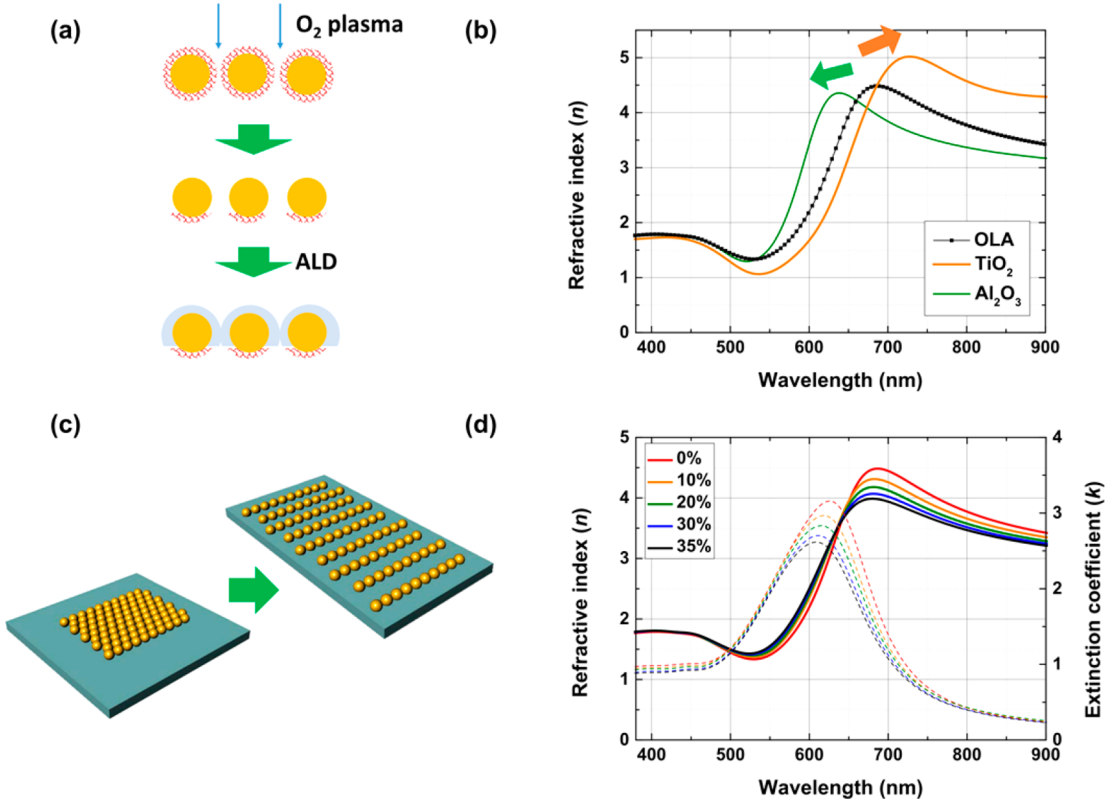

Figure 4. (a) Schematic of encapsulation material substitution to tune the refractive index of the effective optical material by etching and atomic layer deposition (ALD). (b) Effective refractive index of ALD-treated optical material measured by a spectroscopic ellipsometer. The black line with square markers stands for the effective refractive index of an as-fabricated optical material with OLA encapsulation layers. The orange and green lines are the effective refractive indices of samples with 1 nm TiO_2 ALD and 1 nm Al_2O_3 ALD, respectively. (c) Schematic of stretched optical material on a flexible PDMS substrate. (d) Effective refractive index of the stretched optical material measured by a spectroscopic ellipsometer at multiple linear strains.

DOI: 10.1021/acsphotonics.7b01497
ACS Photonics 2018, 5, 1188−1195

polydimethylsiloxane (PDMS) substrate. When the substrate is stretched in one direction, both a and g increase in the same direction and the array becomes anisotropic (Figure 4c).[44] Owing to the positive Poisson's ratio of the substrate, the substrate shrinks in the lateral direction, which decreases a and g in the lateral direction and partially compensates for the stretching effect, but the stretching-induced decrease of the refractive index can be clearly observed experimentally (Figure 4d). It is expected that if the sample is isotropically stretched using air pressure, for example, the resulting optical property would remain isotropic and the change of the refractive index would be greater under the same amount of strain. Additional analysis of the resulting refractive index ellipsoid for anisotropic and isotropic stretching conditions is provided in Supporting Information S10. This mechanical tuning of the index is a reversible process, and the nanoparticle array immediately returns to its original lattice configuration and its optical property is recovered once the tensional force is removed. Thus, it is imaginable that this can be used as a real-time optical sensor for pressure or strain. Here, we used ALD and stretchable substrates to demonstrate the high tunability of the optical properties of the particle array system, but there are other potential tuning modalities as well, such as ligand exchange methods.[29,45]

In this work, we fabricated an effective optical material with close-packed metallic nanoparticle arrays to achieve a tunable refractive index in the visible and infrared wavelength regimes. The measured effective refractive index for the TiO_2-coated gold sphere array is as high as 5.0 near the red part of the visible spectrum, and numerical simulations suggest that the index can reach 7.8 if gold cubes are used. The solution-based fabrication processes used here do not require any top-down lithography or alignment steps and are potentially applicable to large surfaces. We also demonstrated the tunability of the refractive index by both material substitution and mechanical deformation methods. The optical properties measured by spectroscopic ellipsometry are in good agreement with theoretical predictions and numerical calculations. The proposed metal nanoparticle system with considerable index tunability may find applications in diverse areas, such as high-resolution bioimaging, optical lithography, bio- and mechanical sensors, and optical communications.

METHODS

Synthesis of Hydrophobic Gold Nanoparticles and Assembly of a Monolayer of Gold Nanoparticles. A 1 mmol amount of $HAuCl_4 \cdot 3H_2O$ and 10 mmol of oleylamine were added to 50 mL of toluene in a 100 mL flask. The mixture of gold precursor and organic solvents was placed under a nitrogen environment by a reflux system and heated to 105 °C with magnetic stirring. The mixture was kept at 105 °C for 6 h, after which it was cooled to room temperature. A 50 mL amount of ethanol was added to the cooled mixture, and the total mixture was centrifuged at 5000 rpm for 5 min. The solvents were removed, and the centrifuged nanoparticles were dispersed in hexane. The color of the final colloidal solution was red. The synthesized hydrophobic gold nanoparticle was diluted by a solution mixture of toluene and hexane (volume ratio 1:2) as following Wen et al.[5] The glass Petri dish, 145 mm diameter, was three-quarters covered by a glass slide to control the evaporation of the organic solvents. The 600 μL of diluted gold nanoparticle solution was spread on top of the deionized water contained in the glass Petri dish. After evaporation of solvents, a monolayer of gold nanoparticles was fabricated floating on the deionized water.

Spectroscopic Ellipsometer Measurement. The effective refractive index in Figure 2a was measured using a J. A. Woollam M2000D spectroscopic ellipsometer with a 3 mm beam spot size. The effective refractive index in Figures 2b and 4b and d were measured using a J. A. Woollam RC2 spectroscopic ellipsometer with a 50 μm beam spot size. The incident angle was 65 degrees from the surface normal direction for all measurements except in Figure 2, which was measured with three different incident angles of 65, 70, and 75 degrees.

Tunable Effective Index Demonstration by Atomic Layer Deposition and Substrate Stretching. The aluminum oxide (AlO_x) and titanium oxide (TiO_x) were deposited through the ALD method, utilizing trimethyl aluminum and tetrakis(dimethylamido)titanium as metal sources, respectively. Water was used as an oxygen source. The ALD processes were performed at a relatively low temperature of 100 °C to prevent deformation of metallic nanoparticles, and the deposition conditions of the oxide layers were calibrated to be 10 Å based on separate depositions on flat substrates.

In order to stretch the optical material transferred to the PDMS substrates under the spectroscopic ellipsometer setup, a compact stretch tester was custom-built. It was designed to hold a 2 cm by 2 cm sample and stretch it unidirectionally.

FDTD Simulation. Numerical simulations were conducted using a commercial FDTD solver from Lumerical (FDTD Solutions 8.16). All of the FDTD simulations had a three-dimensional computation domain with a minimum mesh size of 0.2 nm. An x-polarized plane wave source with 200 to 2000 nm wavelength range was injected into the simulation domain in the z-direction. A periodic boundary condition was used in the x- and y-directions to implement an infinite array of gold nanoparticles. The array has a finite thickness in the z-direction and perfectly matched layers were used to terminate the z-boundaries. Two planar monitors were placed below and above the array of metal particles to extract the effective material parameters using the S-parameter retrieval method.[46] Using the tabulated optical constants of gold as base values,[47] the size dependence of the permittivity was considered for FDTD calculation.[38]

ASSOCIATED CONTENT

Supporting Information

The Supporting Information is available free of charge on the ACS Publications website at DOI: 10.1021/acsphotonics.7b01497.

Optical microscope and SEM images; raw data of effective refractive index values; numerical calculation results for nanoparticle arrays; AFM measurement results for gold nanoparticle array; effective refractive index of silver nanoparticle array; EDS mapping of cross-section of gold nanoparticle array; numerical calculation result for ALD-treated optical material; numerical calculation of sensitivity for optical material as a refractive index sensor; numerical calculated refractive index of stretched optical material (PDF)

AUTHOR INFORMATION

Corresponding Author

*E-mail: qubit@kaist.ac.kr.

DOI: 10.1021/acsphotonics.7b01497
ACS Photonics 2018, 5, 1188−1195

ORCID
Reehyang Kim: 0000-0002-7643-5604
Jonghwa Shin: 0000-0003-0712-464X

Notes

The authors declare no competing financial interest.

■ ACKNOWLEDGMENTS

This work was supported by the National Research Foundation of Korea (NRF) grant funded by the Korean Government (MSIP) (Nos. 2013M3C1A3063598, 2015R1A5A6001948, 2017R1A2B2005702). This work was also supported by Wearable Platform Materials Technology Center (WMC) funded by the National Research Foundation of Korea (NRF) Grant of the Korean Government (MSIP) (No. 2016R1A5A1009926). The authors declare no competing financial interest.

■ REFERENCES

(1) Yu, H.; Gibbons, P. C.; Kelton, K. F.; Buhro, W. E. Heterogeneous Seeded Growth: A Potentially General Synthesis of Monodisperse Metallic Nanoparticles. *J. Am. Chem. Soc.* **2001**, *123*, 9198.
(2) Chen, M.; Feng, Y.-G.; Wang, X.; Li, T.-C.; Zhang, J.-Y.; Qian, D.-J. Silver Nanoparticles Capped by Oleylamine: Formation, Growth, and Self-Organization. *Langmuir* **2007**, *23*, 5296.
(3) Grzelczak, M.; Pérez-Juste, J.; Mulvaney, P.; Liz-Marzán, L. M. Shape control in gold nanoparticle synthesis. *Chem. Soc. Rev.* **2008**, *37*, 1783.
(4) Reincke, F.; Hickey, S. G.; Kegel, W. K.; Vanmaekelbergh, D. Spontaneous assembly of a monolayer of charged gold nanocrystals at the water/oil interface. *Angew. Chem., Int. Ed.* **2004**, *43*, 458.
(5) Wen, T.; Majetich, S. A. Ultra-large-area self-assembled monolayers of nanoparticles. *ACS Nano* **2011**, *5*, 8868.
(6) Jain, P. K.; Huang, X.; El-Sayed, I. H.; El-Sayed, M. A. Noble metals on the nanoscale: optical and photothermal properties and some applications in imaging, sensing, biology, and medicine. *Acc. Chem. Res.* **2008**, *41*, 1578.
(7) Cho, K.; Wang, X. U.; Nie, S.; Shin, D. M. Therapeutic nanoparticles for drug delivery in cancer. *Clin. Cancer Res.* **2008**, *14*, 1310−1316.
(8) Sau, T. K.; Rogach, A. L.; Jäckel, F.; Klar, T. A.; Feldmann, J. Properties and applications of colloidal nonspherical noble metal nanoparticles. *Adv. Mater.* **2010**, *22*, 1805.
(9) Xia, X.; Tu, J.; Zhang, Y.; Wang, X.; Gu, C.; Zhao, X.-B.; Fan, H. J. High-quality metal oxide core/shell nanowire arrays on conductive substrates for electrochemical energy storage. *ACS Nano* **2012**, *6*, 5531.
(10) Choi, H.; Chen, W. T.; Kamat, P. V. Know thy nano neighbor. Plasmonic versus electron charging effects of metal nanoparticles in dye-sensitized solar cells. *ACS Nano* **2012**, *6*, 4418.
(11) Gilleron, J.; Querbes, W.; Zeigerer, A.; Borodovsky, A.; Marsico, G.; Schubert, U.; Manygoats, K.; Seifert, S.; Andree, C.; Stöter, M.; Epstein-Barash, H.; Zhang, L.; Koteliansky, V.; Fitzgerald, K.; Fava, E.; Bickle, M.; Kalaidzidis, Y.; Akinc, A.; Maier, M.; Zerial, M. Image-based analysis of lipid nanoparticle-mediated siRNA delivery, intracellular trafficking and endosomal escape. *Nat. Biotechnol.* **2013**, *31*, 638.
(12) Fan, J. A.; Bao, K.; Sun, L.; Bao, J.; Manoharan, V. N.; Nordlander, P.; Capasso, F. Plasmonic mode engineering with templated self-assembled nanoclusters. *Nano Lett.* **2012**, *12*, 5318.
(13) Shen, C.; Hui, C.; Yang, T.; Xiao, C.; Tian, J.; Bao, L.; Chen, S.; Ding, H.; Gao, H. Monodisperse Noble-Metal Nanoparticles and Their Surface Enhanced Raman Scattering Properties. *Chem. Mater.* **2008**, *20*, 6939.
(14) Cha, S. K.; Mun, J. H.; Chang, T.; Kim, S. Y.; Kim, J. Y.; Jin, H. M.; Lee, J. Y.; Shin, J.; Kim, K. H.; Kim, S. O. Au−Ag core−shell nanoparticle array by block copolymer lithography for synergistic broadband plasmonic properties. *ACS Nano* **2015**, *9*, 5536.
(15) Riskin, M.; Tel-Vered, R.; Lioubashevski, O.; Willner, I. Ultrasensitive surface plasmon resonance detection of trinitrotoluene by a bis-aniline-cross-linked Au nanoparticles composite. *J. Am. Chem. Soc.* **2009**, *131*, 7368.
(16) Shelby, R. A.; Smith, D. R.; Schultz, S. Experimental Verification of a Negative Index of Refraction. *Science* **2001**, *292*, 77.
(17) Smith, D. R.; Pendry, J. B.; Wiltshire, M. C. K. Metamaterials and Negative Refractive Index. *Science* **2004**, *305*, 788.
(18) Dani, K. M.; Ku, Z.; Upadhya, P. C.; Prasankumar, R. P.; Brueck, S. R. J.; Taylor, A. J. Subpicosecond Optical Switching with a Negative Index Metamaterial. *Nano Lett.* **2009**, *9*, 3565.
(19) Silveirinha, M.; Engheta, N. Tunneling of Electromagnetic Energy through Subwavelength Channels and Bends using ε-Near-Zero Materials. *Phys. Rev. Lett.* **2006**, *97*, 157403.
(20) Edwards, B.; Alu, A.; Young, M. E.; Silveirinha, M.; Engheta, N. Experimental verification of epsilon-near-zero metamaterial coupling and energy squeezing using a microwave waveguide. *Phys. Rev. Lett.* **2008**, *100*, 033903.
(21) Hao, J.; Yan, W.; Qiu, M. Super-reflection and cloaking based on zero index metamaterial. *Appl. Phys. Lett.* **2010**, *96*, 101109.
(22) Shin, J.; Shen, J. T.; Fan, S. Three-dimensional metamaterials with an ultrahigh effective refractive index over a broad bandwidth. *Phys. Rev. Lett.* **2009**, *102*, 093903.
(23) Choi, M.; Lee, S. H.; Kim, Y.; Kang, S. B.; Shin, J.; Kwak, M. H.; Kang, K. Y.; Lee, Y. H.; Park, N.; Min, B. A terahertz metamaterial with unnaturally high refractive index. *Nature* **2011**, *470*, 369.
(24) Chang, T.; Kim, J. U.; Kang, S. K.; Kim, H.; Kim, D. K.; Lee, Y. H.; Shin, J. Broadband giant-refractive-index material based on mesoscopic space-filling curves. *Nat. Commun.* **2016**, *7*, 12661.
(25) Kim, J. Y.; Kim, H.; Kim, B. H.; Chang, T.; Lim, J.; Jin, H. M.; Mun, J. H.; Choi, Y. J.; Chung, K.; Shin, J.; Fan, S. Highly tunable refractive index visible-light metasurface from block copolymer self-assembly. *Nat. Commun.* **2016**, *7*, 12911.
(26) Kubo, S.; Diaz, A.; Tang, Y.; Mayer, T. S.; Khoo, I. C.; Mallouk, T. E. Tunability of the refractive index of gold nanoparticle dispersions. *Nano Lett.* **2007**, *7*, 3418.
(27) Kim, J.; Yang, H.; Green, P. F. Tailoring the refractive indices of thin film polymer metallic nanoparticle nanocomposites. *Langmuir* **2012**, *28*, 9735.
(28) Zhang, H.; Jia, Z.; Lv, X. Surface layer reflective index changes of Au nanoparticle functionalized porous silicon microcavity for DNA detection. *Curr. Appl. Phys.* **2015**, *15*, 870.
(29) Fafarman, A. T.; Hong, S. H.; Caglayan, H.; Ye, X.; Diroll, B. T.; Paik, T.; Engheta, N.; Murray, C. B.; Kagan, C. R. Chemically tailored dielectric-to-metal transition for the design of metamaterials from nanoimprinted colloidal nanocrystals. *Nano Lett.* **2013**, *13*, 350.
(30) Lee, S. Colloidal superlattices for unnaturally high-index metamaterials at broadband optical frequencies. *Opt. Express* **2015**, *23*, 28170.
(31) Tao, A.; Sinsermsuksakul, P.; Yang, P. Tunable plasmonic lattices of silver nanocrystals. *Nat. Nanotechnol.* **2007**, *2*, 435.
(32) López-García, M.; Galisteo-López, J. F.; Blanco, Á.; López, C.; García-Martín, A. High Degree of Optical Tunability of Self-Assembled Photonic-Plasmonic Crystals by Filling Fraction Modification. *Adv. Funct. Mater.* **2010**, *20*, 4338.
(33) Ross, M. B.; Ku, J. C.; Vaccarezza, V. M.; Schatz, G. C.; Mirkin, C. A. Nanoscale form dictates mesoscale function in plasmonic DNA−nanoparticle superlattices. *Nat. Nanotechnol.* **2015**, *10*, 453.
(34) Laxminarayana, G. K.; Rozin, M.; Smith, S.; s Tao, A. R. Modular, polymer-directed nanoparticle assembly for fabricating metamaterials. *Faraday Discuss.* **2016**, *186*, 489.
(35) Ross, M. B.; Mirkin, C. A.; Schatz, G. C. Optical Properties of One-, Two-, and Three-Dimensional Arrays of Plasmonic Nanostructures. *J. Phys. Chem. C* **2016**, *120*, 816.
(36) Masuda, T.; Yamagishi, Y.; Takei, N.; Owaki, H.; Matsusaki, M.; Akashi, M.; Arai, F. Three-Dimensional Assembly of Multilayered Tissues. *Procedia CIRP* **2013**, *5*, 201.

DOI: 10.1021/acsphotonics.7b01497
ACS Photonics 2018, 5, 1188−1195

(37) Chung, K.; Kim, R.; Chang, T.; Shin, J. Optical effective media with independent control of permittivity and permeability based on conductive particles. *Appl. Phys. Lett.* **2016**, *109*, 021114.
(38) Derkachova, A.; Kolwas, K.; Demchenko, I. Dielectric Function for Gold in Plasmonics Applications: Size Dependence of Plasmon Resonance Frequencies and Damping Rates for Nanospheres. *Plasmonics* **2016**, *11*, 941.
(39) Chen, C. F.; Tzeng, S. D.; Chen, H. Y.; Lin, K. J.; Gwo, S. Tunable plasmonic response from alkanethiolate-stabilized gold nanoparticle superlattices: evidence of near-field coupling. *J. Am. Chem. Soc.* **2008**, *130*, 824.
(40) Lewandowski, W.; Fruhnert, M.; Mieczkowski, J.; Rockstuhl, C.; Górecka, E. Dynamically self-assembled silver nanoparticles as a thermally tunable metamaterial. *Nat. Commun.* **2015**, *6*, 6590.
(41) Xu, Z. J.; Zhang, F.; Zhang, R. J.; Yu, X.; Zhang, D. X.; Wang, Z. Y.; Zheng, Y. X.; Wang, S. Y.; Zhao, H. B.; Chen, L. Y. Thickness dependent optical properties of titanium oxide thin films. *Appl. Phys. A: Mater. Sci. Process.* **2013**, *113*, 557.
(42) Groner, M. D.; Elam, J. W.; Fabreguette, F. H.; George, S. M. Electrical characterization of thin Al 2 O 3 films grown by atomic layer deposition on silicon and various metal substrates. *Thin Solid Films* **2002**, *413*, 186.
(43) Chen, X.; Park, H. R.; Pelton, M.; Piao, X.; Lindquist, N. C.; Im, H.; Kim, Y. J.; Ahn, J. S.; Ahn, K. J.; Park, N.; Kim, D. S. Atomic layer lithography of wafer-scale nanogap arrays for extreme confinement of electromagnetic waves. *Nat. Commun.* **2013**, *4*, 2361.
(44) Millyard, M. G.; Min Huang, F.; White, R.; Spigone, E.; Kivioja, J.; Baumberg, J. J. Stretch-induced plasmonic anisotropy of self-assembled gold nanoparticle mats. *Appl. Phys. Lett.* **2012**, *100*, 073101.
(45) Yang, G.; Hu, L.; Keiper, T. D.; Xiong, P.; Hallinan, D. T., Jr Gold nanoparticle monolayers with tunable optical and electrical properties. *Langmuir* **2016**, *32*, 4022.
(46) Smith, D. R.; Schultz, S.; Markoš, P.; Soukoulis, C. M. Determination of effective permittivity and permeability of metamaterials from reflection and transmission coefficients. *Phys. Rev. B: Condens. Matter Mater. Phys.* **2002**, *65*, 195104.
(47) Johnson, P. B.; Christy, R. W. Optical constants of the noble metals. *Phys. Rev. B* **1972**, *6*, 4370.

DOI: 10.1021/acsphotonics.7b01497
ACS Photonics 2018, 5, 1188−1195